Plasmonic resonances in hybrid systems of aluminum nanostructured arrays and few layer graphene within the UV–IR spectral range

IOP Publishing Nanotechnology
Nanotechnology 28 (2017) 465704 (9pp) https://doi.org/10.1088/1361-6528/aa8ce4

Plasmonic resonances in hybrid systems of aluminum nanostructured arrays and few layer graphene within the UV–IR spectral range

R González-Campuzano[1,3], J M Saniger[2] and D Mendoza[1]

[1] Instituto de Investigaciones en Materiales, Universidad Nacional Autónoma de México, A. P. 70-360, Ciudad de México 04510, México
[2] Centro de Ciencias Aplicadas y Desarrollo Tecnológico, Universidad Nacional Autónoma de México, A. P. 70-186, Ciudad de México 04510, México

E-mail: naedra@ciencias.unam.mx and doroteo@unam.mx

Received 27 August 2017, revised 13 September 2017
Accepted for publication 15 September 2017
Published 23 October 2017

Abstract

The size-controllable and ordered Al nanocavities and nanodomes arrays were synthesized by electrochemical anodization of aluminum using phosphoric acid, citric acid and mixture both acids. Few layer graphene (FLG) was transferred directly on top of Al nanostructures and their morphology were evaluated by scanning electron microscopy. The interaction between FLG and the plasmonic properties of Al nanostructures arrays were investigated based on specular reflectivity in the ultraviolet–visible–infrared range and Raman spectroscopy. We found that their optical reflectivity was dramatically reduced as compared with unstructured Al. At the same time pronounced reflectivity dips were detectable in the 200–896 nm wavelength range, which were ascribed to plasmonic resonances. The plasmonic properties of these nanostructures do not exhibit evident changes by the presence of FLG in the UV–vis range of the electromagnetic spectrum. By contrast, the surface-enhanced Raman spectroscopy of FLG was observed in nanocavities and nanodomes structures that result in an intensity increase of the characteristic G and 2D bands of FLG induced by the plasmonic properties of Al nanostructures.

Supplementary material for this article is available online

Keywords: plasmonic nanostructures, aluminum, graphene, SERS, GERS, plasmonic properties, plasmonic aluminum

(Some figures may appear in colour only in the online journal)

1. Introduction

In recent years, the physical and chemical properties of plasmonic [1–3] and two-dimensional materials [4–6] have aroused great interest within the scientific community for their many applications.

Surface plasmons (SPs) are collective oscillations of free charges at the interface between two materials, usually metals and a dielectric material. Control and manipulation of SPs gives us the opportunity to apply them in nanophotonic devices, for example in the confinement of light into nanostructures that are smaller than the wavelength of light, giving novel plasmonic effects such as extraordinary optical transmission in subwavelength hole arrays [7, 8], Fano resonances in metal nanostructures [9], and others.

The use of aluminum in plasmonic nanostructures compared to other noble metals like silver or gold offers new possibilities to access the ultraviolet–visible–infrared (UV–Vis–IR)

[3] Author to whom any correspondence should be addressed.

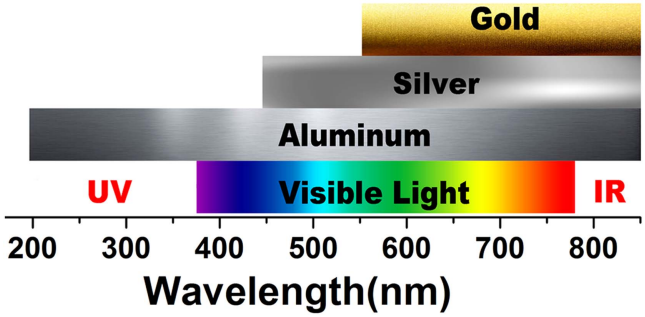

Figure 1. Plasmon tuning ranges of the most common plasmonic materials, Au and Ag, compared with Al.

region of the electromagnetic spectrum (see figure 1), and also by its relatively low cost and high natural abundance.

Recently, due to its high performance Al has been increasingly used in studies and applications in plasmonics, for example as biosensors [10, 11], in surface enhanced fluorescence [12], and surface enhanced Raman scattering (SERS) [13–15].

On the other hand, graphene being a bidimensional material of atomic thickness (0.34 nm) [16] has attracted a lot of attention in different areas of science for its interesting optical [17], thermal [18], electronic [19] and phononic [20] properties. Currently, there are some reports on graphene deposited on thin metal films to be used as a biosensor based on surface plasmons resonance (SPR) [21], furthermore, recent studies show that this material possesses plasmonic properties [22], especially at mid-infrared (MIR) [23] and terahertz (THz) [24] frequencies. With these motivations and combining plasmonic properties of Al nanostructures and graphene, systems with novel properties can be obtained. For example, such hybrid systems could be promising for Raman enhancement phenomenon known as graphene-enhanced Raman scattering (GERS) [25–27], where at the same time SERS phenomena is present.

In this work, we propose and fabricate a novel system based on few layer graphene (FLG) on top of ordered and size-controlled Al nanostructures (nanocavity and nanodome arrays) to study the light–matter interaction in graphene−plasmonic hybrid structures. We used electrochemical anodization to synthesize the nanostructures. FLG synthesized by a chemical vapor deposition (CVD) method was transferred directly on top of Al nanostructures and their interaction with plasmonic Al nanostructures were investigated through reflectance and Raman spectroscopy measurements. We found that plasmon resonances are excited both in nanocavities and in nanodomes arrays, and that the presence of FLG does not significantly affect the plasmonic properties of these nanostructures in the UV–vis range of the electromagnetic spectrum. On the other hand, we observed a SERS effect where Raman intensities of both G and 2D bands of FLG enhanced when it is on top of the nanostructures.

2. Experimental details

High-purity aluminum foil (Sigma-Aldrich 0.25 mm thick, 99.999% purity) was cut in 1 cm × 2.5 cm samples. Before the anodization process the Al foils were annealed at 600 °C for 6 h in an atmosphere of H_2 at ambient pressure. Subsequently they were cleaned in solutions of 0.25 M Na_2CO_3 at 80 °C for 3 min and 35% wt HNO_3 for 30 s. Various kinds of samples using phosphoric acid (H_3PO_4), citric acid ($C_6H_8O_7$) and mixture both acids [28] as electrolytes for anodization were obtained (see supplementary material available online at stacks.iop.org/NANO/28/465704/mmedia); voltages in the range of 130–600 V were applied at ambient temperature for 8 h. A graphite plate was used as the counter electrode and the distance between both electrodes was kept 1 cm apart; the solutions were continuously stirred to homogenize both the electrolyte and its temperature.

After anodizing, the samples were immersed in a mixture of 1.8 wt% CrO_3 and 6 wt% H_3PO_4 at 60 °C for 12 h to selectively dissolve the anodic aluminum oxide (AAO), with this procedure an array of concaves is observed in the remaining aluminum surface, see figure 2(a).

Other type of plasmonic structures denominated nanodomes were also explored (see figure 2(b)), namely the bottom surface, called the barrier layer of the AAO was used as a substrate where a thin aluminum film was evaporated (see supplementary material).

Carbonaceous material was synthesized by CVD method using the same procedure reported in [29]. Briefly, for annealing, copper foil was heated to 1000 °C with flowing H_2 during one and a half hour. After this time a gas mixture of H_2 and CH_4 was flowed at ambient pressure for 30 min. Flowing CH_4 was cut off and the furnace was cooled to room temperature in the H_2 atmosphere. Under these conditions of synthesis few layers of graphene were obtained. Cooper foil was dissolved in solution of $Fe(NO_3)_3$, and FLG was transferred on Al nanostructured arrays for optical measurements.

Morphology of the nanostructured Al arrays samples was evidenced by using field-emission scanning electron microscope (SEM) JEOL 7600F. Reflectivity measurement was performed using UV–vis spectrophotometer (UV-2600 Shimadzu Corporation). The probe was set at normal angle and reflectance spectra were collected using integrating sphere in the 190–1400 nm wavelength range. Raman spectroscopy was made using Nicolet Almega XR Spectrometer with 532 nm laser excitation, and 0.784 mW of laser power.

3. Results and discussion

After anodization and thorough removal of the resulting AAO, an array of concaves appears on the Al sample, which is an exact replica of the morphology of the AAO pore bottoms. In figure 3 representative top view SEM images of Al nanocavities arrays synthesized at different voltages are shown.

The geometric parameters such as interconcave distance (D_c) and pore concave diameter (D_p) of these nanostructures were estimated from SEM micrographs for each sample using Image J software. The determined values are presented in table S2 of supplementary material. As can be seen in figure 4, the size of these nanostructures depends on the

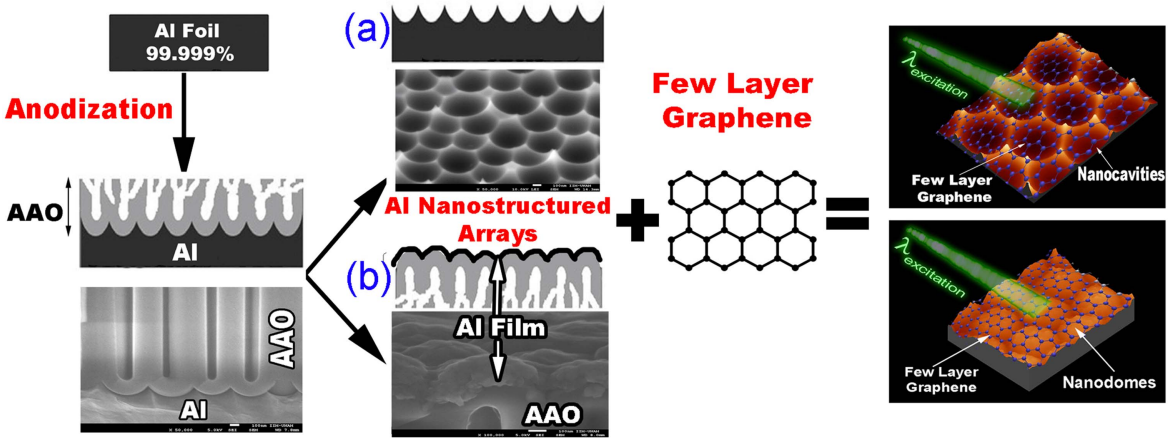

Figure 2. Schematic representation of the experimental procedure for the synthesis of hybrid systems.

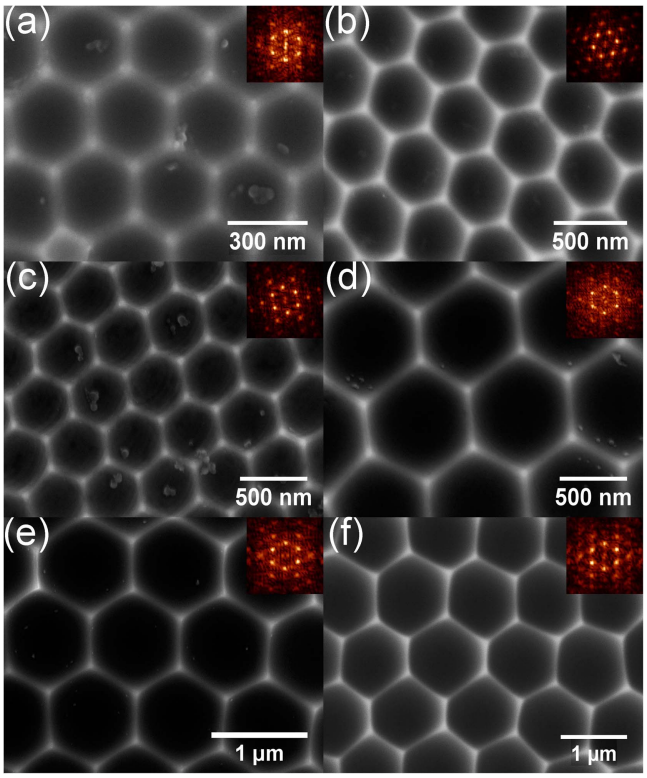

Figure 3. Some SEM micrographs of Al nanocavities arrays fabricated with different voltages: (a) 130 V, (b) 160 V, (c) 180 V, (d) 300 V, (e) 350 V and (f) 400 V with their respective FFT images (insets).

applied voltage, keeping an impressive linear relation between both parameters and the anodization voltage. That is why the process of electrochemical anodization, compared to other expensive techniques such as lithography, is a good alternative because it is possible to obtain desired dimensions by choosing the appropriate electrolyte and anodization voltage. An FFT analysis was also performed from SEM micrographs, shown six distinct points in the corners of a hexagon, confirming good hexagonal arrangement of the nanostructures (see upper inset of figure 3).

Reflectance spectrums as a function of light wavelength of some Al nanostructures are shown in figure 5. A significant

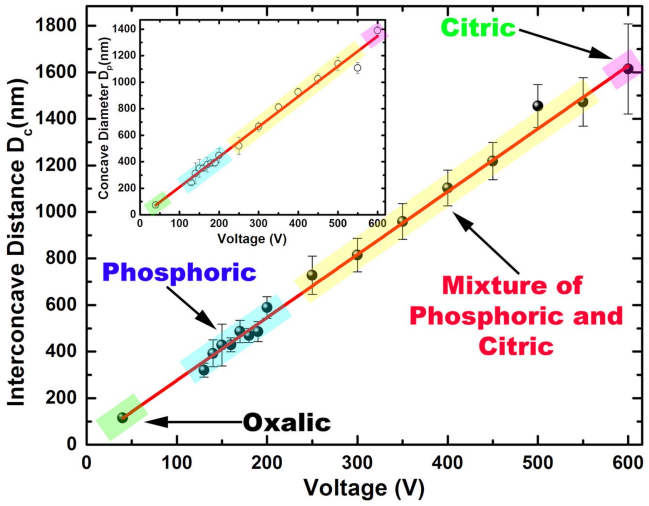

Figure 4. The relation between the interconcave distance (D_c), pore concave diameter (D_p, inset) and the applied anodizing voltage in nanocavities arrays for different acidic electrolytes used in this work.

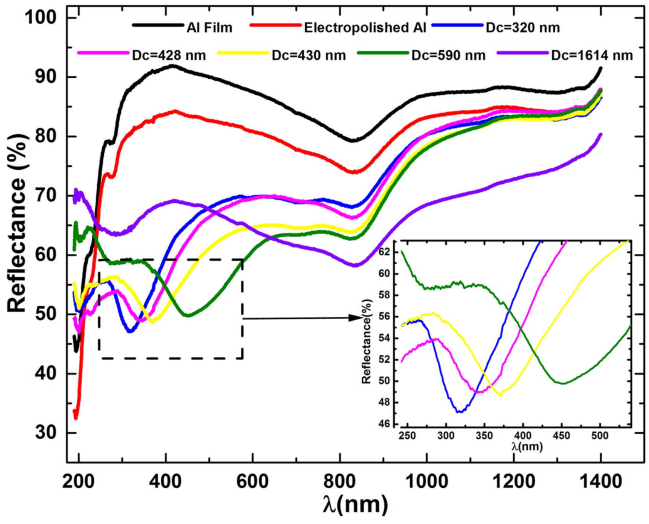

Figure 5. Reflectance spectrum of Al nanocavities. Results for electropolished Al foil and Al film obtained by thermal evaporation are shown for comparison.

dip in the reflectance intensity at 826 nm (~1.5 eV) is observed in all cases. This feature is related with interband transitions of electrons in the crystalline aluminum [30, 31]. In the samples with nanocavities arrays with D_c within the 320–728 nm range other dip in the reflectance in the 300–538 nm wavelength range appears (inset figure 5), while in samples with D_c in the 814–1614 nm range this dip is not evident. The SPs excitations manifest themselves as minima in reflectance spectrum in UV–visible region [32], which means that the incident light couples with SPs located at Al nanocavities array.

It is observed that while D_c increases, the plasmon dip moves to longer wavelengths, and when it approaches to the reflectance minima related with interband transitions of Al, the existence of the plasmonic dip is no longer evident. The interband transitions cause damping of any localized surface plasmon resonances (LSPRs) or propagating surface plasmon polaritons (SPPs) that have energies matching those of the interband transitions [33], hence a competitive phenomena between interband transitions and SPs excitations appears [34].

The nanocavities arrays provide the additional momentum $\vec{G}$ necessary to fulfill the resonance conditions, giving rise to the dips in reflectance spectra [8, 32]. The SP resonances are directly associated with the periodicity of the nanocavities arrays and to the optical properties of Al. Using as a first approximation for SPR an ideal model, coupling of photons with two-dimensional hexagonal periodic array gives SPR or minimum of the reflectance at the wavelength given by [8, 35]:

$$\lambda_{\mathrm{SPR}} = \frac{a}{\sqrt{\frac{4}{3}(i^2 + ij + j^2)}} \sqrt{\frac{\varepsilon_m(\lambda)\varepsilon_d}{\varepsilon_m(\lambda) + \varepsilon_d}} \qquad (1)$$

at normal incidence, where a is the period of the array (in our case interconcave distance D_c), ε_m and ε_d are respectively the dielectric constants of the metal and the dielectric material in contact with the metal and i, j are the scattering orders of the array; in this model variations in metal thickness, the size and shape of the nanostructures are not taken into account. Although the equation (1) was developed for periodic arrays, to generate the SPR a long-range order is not necessary [32].

The most pronounced dips in the reflectance spectra can be ascribed to the $(i, j) = (1, 0)$ or first order ($\lambda_{(1,0)}$) according to equation (1). A second dip present in some spectra of Al nanocavities synthetized with different voltages may be attributed to a higher order SPR mode $(i, j) = (1, 1)$ or second order ($\lambda_{(1,1)}$). Figure 6 shows experimental data of the observed reflectance dips and theoretical curve for the SP resonance model with periodicity described by equation (1).

For calculations, the real part of equation (1) was solved using experimental values for the complex dielectric function of Al [36] $\varepsilon_m(\lambda) = \varepsilon_1 + \mathrm{i}\varepsilon_2$ taking $\varepsilon_d = 1$ for air. It is observed in figure 6 that the analytical curves for the $\lambda_{(1,0)}$ and $\lambda_{(1,1)}$ modes fit acceptably to the experimental reflectance dips within the 320–728 nm range of D_c. In a previous report [37] we showed that the periodicity is not essential for the excitation of SPs in this range of D_c values and that the irregularity on the surface is the important characteristic for the momentum conservation rule [32].

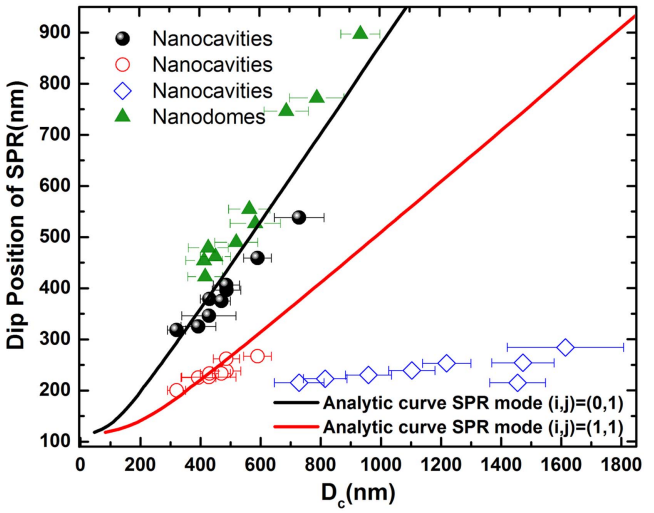

Figure 6. Comparison of experimental data dip for Al nanocavities arrays (open and closed circles), Al nanodomes arrays (closed triangles) and analytical curves for the SPR model for the fundamental modes $(i, j) = (0, 1)$ and $(i, j) = (1, 1)$. Other dips appeared in the nanocavities arrays are shown as open diamonds.

The discrepancy in the fit may be related with the formation of native layer of alumina (Al_2O_3) (~3–5 nm) that appears on the surface of Al when exposed to air which acts as a passivation layer preventing further oxidation. Oxidation in Al nanostructures has been thoroughly studied [38–40], and established that the plasmonic response of Al is remarkably sensitive to the percentage of oxide. In others works [41, 42] it is proposed that the discrepancy with the model may be attributed to the fact that the nanocavities are ended by very sharp edges which can support LSPRs and that the interaction between SPP and LSP modes can cause shifts in minima corresponding to SP excitations.

There are other reflectance dips (diamond open symbols in figure 6), which appear on samples with D_c values higher than 728 nm. Note that these dips completely separate of the tendency of the analytical curves. Our proposal is that these dips are related to other type of electromagnetic modes, namely cavity modes, in this case light is confined within the cavity as standing waves [43, 44]; but these findings deserve further careful investigation.

On the other side, FLG was put on the nanocavity arrays to study the interaction between both systems in two cases: the effect of FLG on the position of the plasmon resonances of the arrays and the changes on the Raman bands of FLG produced by the nanocavities substrates.

In the first case, reflectance spectrums as a function of light wavelength of the Al nanocavities with FLG are shown in figure 7(a). A significant dip in the reflectance intensity at 269 nm (~4.6 eV) is observed in all samples in addition to the minima corresponding to SPR. The minimum around 269 nm corresponds to FLG and is associated to the optical transition $\pi \rightarrow \pi^*$ (~4.5–4.6 eV) in graphene [45], such as is evident in

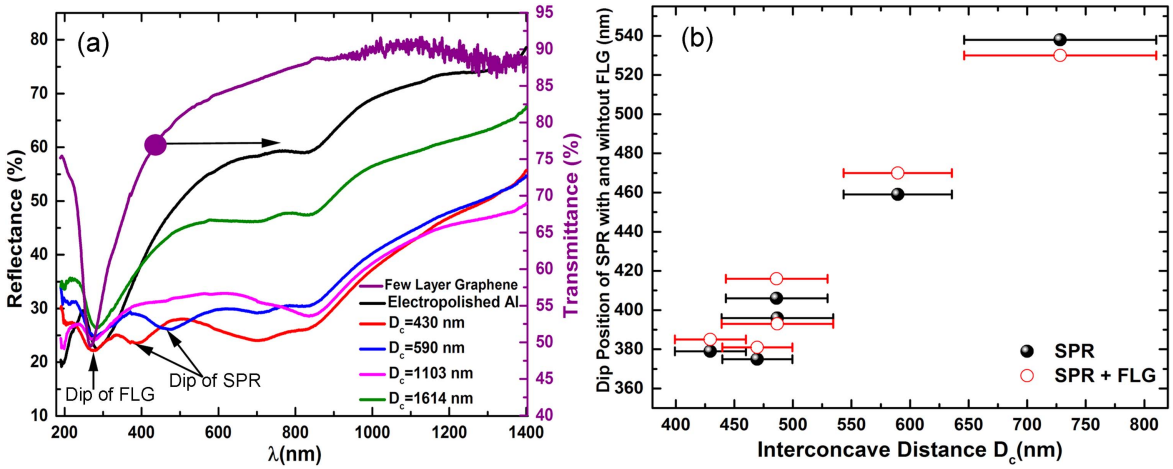

Figure 7. (a) Reflectance spectrum of FLG on top on Al nanocavities. Results for electropolished Al foil with FLG and transmittance spectrum of FLG are shown for comparison. (b) Comparison of plasmonic minima of Al nanocavities (closed symbols) and Al nanocavities with FLG (open symbols).

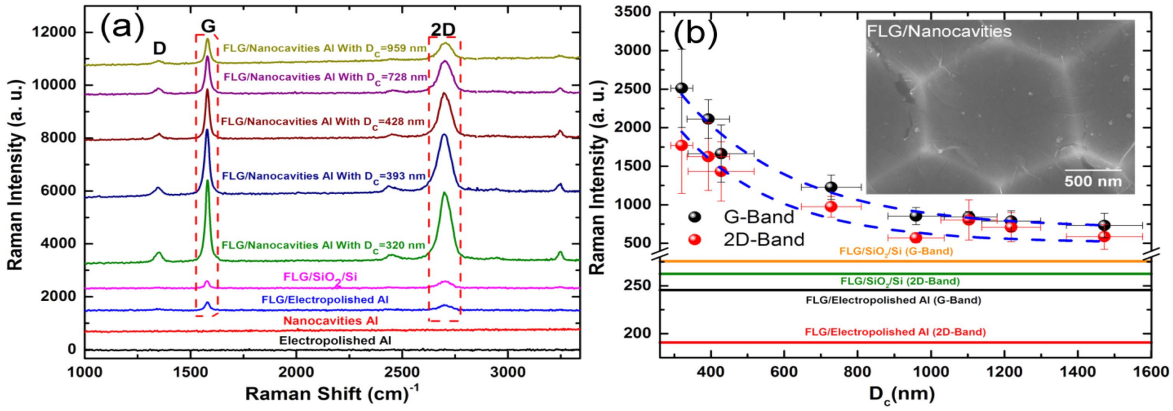

Figure 8. (a) Comparison of Raman spectra of FLG on the surface of the nanocavities with different D_c. Results for electropolished Al foil, nanostructured Al (with nanocavities), FLG on top of SiO_2 (306 nm)/Si and electropolished Al are shown for comparison. All the measurements were performed using a excitation laser wavelength of 532 nm, with a 10× objective (spot size ∼5 μm) and 0.784 mW incident power. (b) Raman intensity changes for the G and 2D band depending on the D_c of nanocavities. The horizontal lines show the Raman intensity of substrates used as reference. SEM image of FLG on top of Al nanocavities arrays (inset).

the transmittance measurements of FLG on quartz substrate shown in the same figure.

Figure 7(b) shows the position of the first order plasmonic minima in the reflectance intensity of nanocavities with and without FLG. Our experimental results do not show any evident systematic change on the plasmonic resonances of the Al nanocavities when FLG is put on these substrates. But an overall decrease of the reflectance intensity after placing FLG on top of Al nanocavities is observed, which can be ascribed to the absorption of the graphene layers [17].

In the second case, Raman spectroscopy was used to sense the effect of Al nanocavities in FLG. A detailed analysis of the shape of the 2D band of Raman spectrum (see supplementary material) showed that the samples consisted of four layers of graphene, which is consistent with the value of the measured transmittance in the visible range using the general rule of 2.3% of absorbance per graphene layer as is shown in the transmittance spectrum of figure 7(a).

In figure 8(a) Raman spectra of electropolished Al, nanostructured Al (with nanocavities), FLG on top of SiO_2 (306 nm)/Si, on electropolished Al and on Al nanocavities with different D_c as substrates are shown. The spectrums of the systems used as references (electropolished and nanostructured Al) do not present any Raman band within the 1350–3500 cm^{-1} range, while FLG present their characteristic D, G and 2D bands. Note that the intensity of the G band is larger than that of the 2D band, which is characteristic of the FLG samples.

We observe in figure 8(b) that Raman signal intensity of the characteristic G and 2D peaks of FLG significantly increases when is on top of Al nanocavities with different D_c in comparison with substrates used as references. At the lower D_c, FLG on top of Al nanocavities display an enhancement factor of ∼10-fold for the G peak and ∼9 for the 2D peak compared to FLG on top of electropolished Al and ∼9-fold for the G peak and ∼7-fold for the 2D peak compared to FLG on top of SiO_2/Si. This fact may be related to a SERS effect produced by the nanocavities arrays.

The decreasing behavior in the Raman signal intensity as a function of D_c can be directly related with the number of

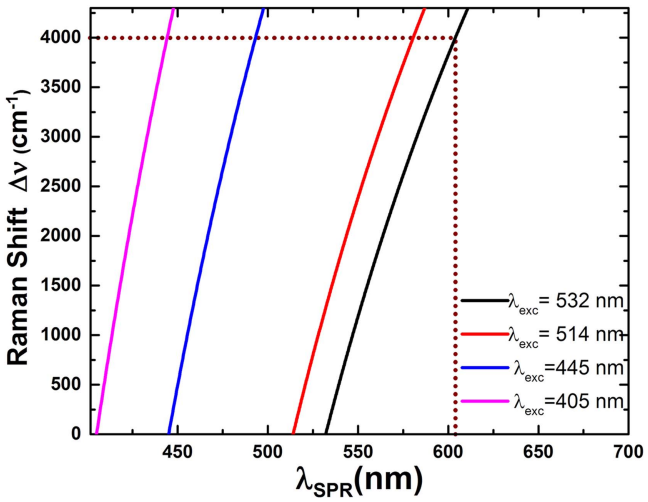

Figure 9. Raman shift ($\Delta\nu$) as a function of wavelength of the SPR (λ_{SPR}) for different excitation wavelengths (λ_{exc}) commonly used in Raman spectroscopy.

nanocavities per unit area or so-called hotspots. The hot spots are highly localized regions of intense local field enhancement believed to be caused by SPR [46].

It is known that the SERS enhancement is strongly related to the plasmonic properties of the nanostructures and that the maximum enhancement is achieved when the wavelength of the SPR of the nanostructure (λ_{SPR}) (in our case Al nanocavities) is located between the excitation wavelength (λ_{exc}) and the wavelength of Raman signal (λ_{RS}) of analyte [47] (in our case FLG).

Theoretical and experimental results [48–52] demonstrated that the maximum enhancement occurs when the λ_{SPR} is equal to the average of the λ_{exc} and the λ_{RS}; that is:

$$\lambda_{SPR} = \frac{\lambda_{exc} + \lambda_{RS}}{2}. \quad (2)$$

Using equation (2) we can obtain an expression that allows us to calculate the Raman shift ($\Delta\nu$) from the known parameters λ_{SPR} and λ_{exc}:

$$\Delta\nu = \frac{1}{\lambda_{exc}} - \frac{1}{2\lambda_{SPR} - \lambda_{exc}}. \quad (3)$$

Figure 9 shows the calculated Raman shift ($\Delta\nu$) as a function of wavelength of the SPR (λ_{SPR}) for different excitation wavelengths (λ_{exc}). The advantage of using Al nanocavities as SERS substrates is that one can change λ_{SPR} at will by applying the selected anodization voltage (see figures 4 and 6), and with the appropriate λ_{exc} it is possible perform Raman studies of analytes in any desired wavenumbers region. The maximum Raman shift, even in the so called high wavenumber Raman spectroscopy [53, 54], is 4000 cm^{-1}; then, using the results presented in figure 9, one can choose the appropriate parameters for SERS characterization.

A limitation of Al nanocavities arrays to be used as SERS substrates in regions smaller than 4000 cm^{-1} with an excitation wavelength of 532 nm (used in this work) is that λ_{SPR} should be located between 532 and 604 nm according to figure 9. The experimental results obtained in the present study indicated that λ_{SPR} is limited to a maximum of around 538 nm (see figure 6). Due to this limitation, it is explored the other kind of plasmonic nanostructures denominated nanodomes (see figures 2(b), 10(a) and supplementary material for details of fabrication).

Figure 10(b) shows the reflectance spectra of Al nanodomes arrays. The dip in the reflectance intensity related with interband transitions in Al around 826 nm in these nanostructures is less evident compared to Al nanocavities arrays. In addition, minima in the UV–visible region in the range of 422–896 nm corresponding to SPs excitations are also observed (see figure 6), where an acceptable fit of the theoretical curve with the experimental results is observed. Due to this wide range of plasmonic resonances, and according to figure 9, Al nanodomes arrays may be better candidates to be used as SERS substrates in comparison to Al nanocavities using an excitation light with 532 nm wavelength.

In figure 10(c) Raman spectra of FLG on top of Al nanodomes arrays with different D_c as substrates are shown. It is also observed that Raman signal intensity of the characteristic peaks of FLG significantly increased when is on top of Al nanodomes arrays with different D_c in comparison with substrates used as references. Figure 10(d) shows Raman signal intensities changes for the G and 2D bands of FLG when is on top of Al nanodomes arrays with different D_c. For the minimum value of D_c explored in this work, FLG on top of Al nanodomes arrays display enhancement factors of ~15-fold for the G peak and 16 for the 2D peak compared to FLG on top of unstructured Al and ~13-fold for the G peak and ~12-fold for the 2D peak compared to FLG on top of SiO_2/Si. This type of nanostructures show enhancement factors in G and 2D peaks greater than those of the Al nanocavities arrays. This fact may be related to the more complex geometry of this system that includes the thickness of the Al film and the surrounding dielectric media or to a texture that naturally appears in the Al film deposited on the nanodomes (see figures 10(a) and S1).

Using the plasmonic properties of the Al nanocavities arrays and the extended SPR spectral range of Al nanodomes arrays, it is possible to design SERS substrates similar to those reported in [55, 56], formed by FLG and metallic nanostructures combinations called graphene-mediated SERS (G-SERS) substrate. Some advantages of graphene on top of Al nanocavities and Al nanodomes arrays are: can act as a multifunctional 'SERS mediator', a flat supporting surface to arrange molecules in a more controllable way, a spacer to separate the metal-molecule contact, additional effects like a stabilizer of both the substrate and the molecules under laser exposure; so this G-SERS substrate may be superior of others typical SERS substrates. In addition, graphene presents by itself an enhanced Raman effect (GERS) [29].

4. Conclusions

In summary, these nanostructures are simple to fabricate compared to other expensive techniques such as lithography

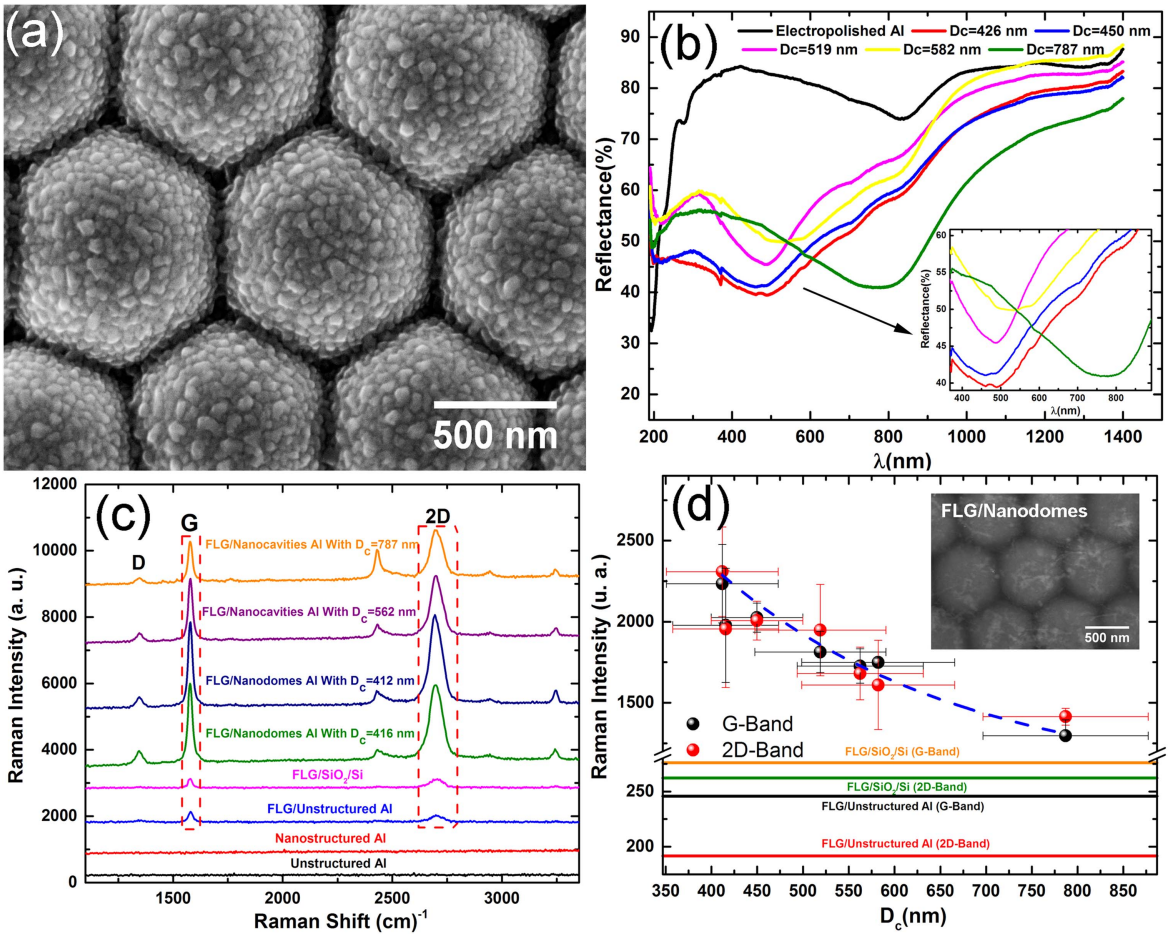

Figure 10. (a) SEM image of top view of Al nanodomes arrays. (b) Reflectance spectrum of Al nanodomes arrays. (c) Comparison of Raman spectra of FLG on the surface of the Al nanodomes arrays with different D_c. Results for unstructured Al foil, nanostructured Al, FLG on top of SiO_2 (306 nm)/Si and unstructured Al are shown for comparison. All the measurements were performed using the same conditions as in figure 8(a). (d) Raman intensity changes for the G and 2D band depending on the D_c of Al nanodomes arrays. The horizontal lines show the Raman intensity of substrates used as reference.

and their plasmonic properties can easily be tuned by changing their size through the appropriate electrolyte and anodization voltage. These characteristics combined with the properties of multilayer graphene can offer great promise for their use in GERS–SERS studies for sensing and characterization of biological and chemical molecules. Although the plasmonic properties of Al nanocavities, compared to other metals such as Au and Ag, are limited in wavelength regions smaller than 830 nm because of interband transitions, that system can be useful in the ultraviolet–visible wavelength range. But the nanodomes nanostructures offer an alternative for higher wavelengths and then expanding to the UV–Vis–IR region of the electromagnetic spectrum.

Acknowledgments

We thank Dra Ma Esther Mata (CCADET-UNAM) for her assistance in the synthesis of Al nanostructures, Josué E Romero (IIM-UNAM) for SEM images, Miguel A Canseco (IIM-UNAM) for his assistance in the UV–Vis equipment, Professor Stephen Muhl of IIM-UNAM for his laboratory facilities, Dra Claudia Bautista (CCADET-UNAM) for her suggestions in the analysis of the Raman spectra, Raúl Reyes of IIM-UNAM for his technical support and finally to Laboratorio Universitario de Caracterización Espectroscópica (LUCE-CCADET-UNAM) for facilities in Raman characterization.

ORCID iDs

R González-Campuzano https://orcid.org/0000-0003-2783-3961

References

[1] Liu Z, Fu G, Huang Z, Chen J, Pan P, Yang Y X and Liu Z M 2017 Aluminum and silicon hybrid nano-cavities for four-band, near-perfect light absorbers *Mater. Lett.* **194** 13–5

[2] Jiang D and Yang W 2017 Refractory material based frequency selective emitters/absorbers for high efficiency and thermal stable thermophotovoltaics *Sol. Energy Mater. Sol. Cells* **163** 98–104

[3] Shevchenko K G, Cherkasova V R, Tregubov A A, Nikitin P I and Nikitin M P 2017 Surface plasmon resonance as a tool for investigation of non-covalent nanoparticle interactions in heterogeneous self-assembly & disassembly systems *Biosens. Bioelectron.* **88** 3–8

[4] Liu Y, Bartal G and Zhang X 2008 All-angle negative refraction and imaging in a bulk medium made of metallic nanowires in the visible region *Opt. Express* **16** 15439–48

[5] Yao J, Liu Z, Liu Y, Wang Y, Sun C, Bartal G, Stacy A M and Zhang X 2008 Optical negative refraction in bulk metamaterials of nanowires *Science* **321** 930

[6] Zhu A Y, Kuznetsov A I, Luk'yanchuk B, Engheta N and Genevet P 2017 Traditional and emerging materials for optical metasurfaces *Nanophotonics* **6** 452–71

[7] Ebbesen T W, Lezec H J, Ghaemi H F, Thio T and Wolff P A 1998 Extraordinary optical transmission through sub-wavelength hole arrays *Nature* **391** 667–9

[8] Genet C and Ebbesen T W 2007 Light in tiny holes *Nature* **445** 39–46

[9] Miroshnichenko A E, Flach S and Kivshar Y S 2010 Fano resonances in nanoscale structures *Rev. Mod. Phys.* **82** 2257

[10] Li W, Qiu Y, Zhang L, Jiang L, Zhou Z, Chen H and Zhou J 2016 Aluminum nanopyramid array with tunable ultraviolet–visible–infrared wavelength plasmon resonances for rapid detection of carbohydrate antigen 199 *Biosens. Bioelectron.* **79** 500–7

[11] Liu C S, Sun C X, Tian J Y, Wang Z W, Ji H F, Song Y, Zhang S, Zhang Z H, He L H and Du M 2017 Highly stable aluminum-based metal-organic frameworks as biosensing platforms for assessment of food safety *Biosens. Bioelectron.* **91** 804–10

[12] Chowdhury M H, Ray K, Gray S K, Pond J and Lakowicz J R 2009 Aluminum nanoparticles as substrates for metal-enhanced fluorescence in the ultraviolet for the label-free detection of biomolecules *Anal. Chem.* **81** 1397–403

[13] Zhang X, Zhao J, Whitney A V, Elam J W and Van Duyne R P 2006 Ultrastable substrates for surface-enhanced Raman spectroscopy: Al_2O_3 overlayers fabricated by atomic layer deposition yield improved anthrax biomarker detection *J. Am. Chem. Soc.* **128** 10304–9

[14] Martinez-Garcia M M, Cardoso-Avila P E and Pichardo-Molina J L 2016 Concave gold nanocubes on Al-6063 alloy as a simple and efficient SERS substrate *Colloids Surf.* A **493** 66–73

[15] Sharma B, Cardinal M F, Ross M B, Zrimsek A B, Bykov S V, Punihaole D, Asher S A, Schatz G C and Van Duyne R P 2016 Aluminum film-over-nanosphere substrates for deep-UV surface-enhanced resonance Raman spectroscopy *Nano Lett.* **16** 7968–73

[16] Geim A K and Novoselov K S 2007 The rise of graphene *Nat. Mater.* **6** 183–91

[17] Nair R R, Blake P, Grigorenko A N, Novoselov K S, Booth T J, Stauber T, Peres N M R M R and Geim A K 2008 Fine structure constant defines visual transparency of graphene *Science* **320** 1308

[18] Balandin A A, Ghosh S, Bao W, Calizo I, Teweldebrhan D, Miao F and Lau C N 2008 Superior thermal conductivity of single-layer graphene *Nano Lett.* **8** 902–7

[19] Novoselov K S, Geim A K, Morozov S V, Jiang D, Katsnelson M I, Grigorieva I V, Dubonos S V and Firsov A A 2005 Two-dimensional gas of massless Dirac fermions in graphene *Nature* **438** 197–200

[20] Pandya A and Jha P K 2017 Electron transport parameters study for transition metal-doped armchair graphene nanoribbon via acoustical phonon interactions *J. Electron. Mater.* **46** 2340–6

[21] Szunerits S, Maalouli N, Wijaya E, Vilcot J P and Boukherroub R 2013 Recent advances in the development of graphene-based surface plasmon resonance (SPR) interfaces *Anal. Bioanal. Chem.* **405** 1435–43

[22] Grigorenko A N, Polini M and Novoselov K S 2012 Graphene plasmonics *Nat. Photon.* **6** 749–58

[23] Fei Z *et al* 2012 Gate-tuning of graphene plasmons revealed by infrared nano-imaging *Nature* **487** 82–5

[24] D'Apuzzo F, Piacenti A R, Giorgianni F, Autore M, Guidi M C, Marcelli A, Schade U, Ito Y, Chen M and Lupi S 2017 Terahertz and mid-infrared plasmons in three-dimensional nanoporous graphene *Nat. Commun.* **8** 14885

[25] Huang S, Ling X, Liang L, Song Y, Fang W, Zhang J, Kong J, Meunier V and Dresselhaus M S 2015 Molecular selectivity of graphene-enhanced Raman scattering *Nano Lett.* **15** 2892–901

[26] Zhang N, Tong L and Zhang J 2016 Graphene-based enhanced raman scattering toward analytical applications *Chem. Mater.* **28** 6426–35

[27] Ling X, Wu J, Xie L and Zhang J 2013 Graphene-thickness-dependent graphene-enhanced Raman scattering *J. Phys. Chem.* C **117** 2369–76

[28] Chen X, Yu D, Cao L, Zhu X, Song Y, Huang H, Lu L and Chen X 2014 Fabrication of ordered porous anodic alumina with ultra-large interpore distances using ultrahigh voltages *Mater. Res. Bull.* **57** 116–20

[29] Bautista-Flores C, Sato-Berrú R Y and Mendoza D 2014 Charge transfer in the fullerene C60-few layer graphene system and the existence of negative photoconductivity *Appl. Phys. Lett.* **105** 191116

[30] Hughes A J, Jones D and Lettington A H 1969 Calculation of the optical properties of aluminium *J. Phys. C: Solid State Phys.* **2** 102–3

[31] Ehrenreich H, Philipp H R and Segall B 1963 Optical properties of aluminum *Phys. Rev.* **132** 1918–28

[32] Raether H 1988 Surface plasmons on smooth and rough surfaces and on gratings *Springer Tracts in Modern Physics* vol 111 (Berlin: Springer)

[33] De Silva K S B, Keast V J, Gentle A and Cortie M B 2017 Optical properties and oxidation of α-phase Ag–Al thin films *Nanotechnology* **28** 095202

[34] Maier S A 2007 *Plasmonics: Fundamentals and Applications* (Berlin: Springer)

[35] Papaioannou E T, Kapaklis V, Melander E, Hjörvarsson B, Pappas S D, Patoka P, Giersig M, Fumagalli P, Garcia-Martin A and Ctistis G 2011 Surface plasmons and magneto-optic activity in hexagonal Ni anti-dot arrays *Opt. Express* **19** 23867–77

[36] Palik E D 1985 *Handbook of Optical Constants of Solids* vol 2 (New York: Academic)

[37] Gonzalez-Campuzano R and Mendoza D 2017 Plasmonic resonances in ordered and disordered aluminum nanocavities arrays *J. Phys.: Conf. Ser.* **792** 012077

[38] Knight M W, King N S, Lifei L, Everitt H O, Nordlander P and Halas N J 2014 Aluminum for plasmonics *ACS Nano.* **8** 834–40

[39] Ayas S, Topal A E, Cupallari A, Güner H, Bakan G and Dana A 2014 Exploiting native Al_2O_3 for multispectral aluminum plasmonics *ACS Photon.* **1** 1313–21

[40] Chan G H, Zhao J, Schatz G C and Van Duyne R P 2008 Localized surface plasmon resonance spectroscopy of triangular aluminum nanoparticles *J. Phys. Chem.* C **112** 13958–63

[41] Norek M, Włodarski M and Matysik P 2014 UV plasmonic-based sensing properties of aluminum nanoconcave arrays *Curr. Appl. Phys.* **14** 1514–20

[42] Norek M, Włodarski M and Stepniowski W J 2014 Tailoring of UV/violet plasmonic properties in Ag, and Cu coated Al concaves arrays *Appl. Surf. Sci.* **314** 807–14

[43] Kang G, Wang J, Li P, Zang J, Meng X and Tan X 2016 Modes manipulation within subwavelength metallic gratings *Plasmonics* **11** 1169–74

[44] Sun G and Zheng J 2005 Investigation of some electromagnetic modes in the metal-dielectric system by the absorption spectrum *Sci. Technol. Adv. Mater.* **6** 848–54
[45] Bulusheva L G, Sedelnikova O V and Okotrub A V 2016 Many-body effects in optical response of graphene-based structures *Int. J. Quantum Chem.* **116** 270–81
[46] Kumar C S S R 2012 *Raman Spectroscopy for Nanomaterials Characterization* (New York: Springer)
[47] Haynes C L, Yonzon C R, Zhang X and Van Duyne R P 2005 Surface-enhanced Raman sensors: early history and the development of sensors for quantitative biowarfare agent and glucose detection *J. Raman Spectrosc.* **36** 471–84
[48] Kahraman M, Daggumati P, Kurtulus O, Seker E and Wachsmann-Hogiu S 2013 Fabrication and characterization of flexible and tunable plasmonic nanostructures *Sci. Rep.* **3** 3396
[49] Grand J, Lamy de la Chapelle M, Bijeon J-L, Adam P-M, Vial A and Royer P 2005 Role of localized surface plasmons in surface-enhanced Raman scattering of shape-controlled metallic particles in regular arrays *Phys. Rev.* B **72** 033407
[50] Haynes C L and Van Duyne R P 2003 Plasmon-sampled surface-enhanced Raman excitation spectroscopy *J. Phys. Chem.* B **107** 7426–33
[51] Félidj N, Aubard J, Lévi G, Krenn J R, Salerno M, Schider G, Lamprecht B, Leitner A and Aussenegg F R 2002 Controlling the optical response of regular arrays of gold particles for surface-enhanced Raman scattering *Phys. Rev.* B **65** 075419
[52] McFarland A D, Young M A, Dieringer J A and Van Duyne R P 2005 Wavelength-scanned surface-enhanced Raman excitation spectroscopy *J. Phys. Chem.* B **109** 11279–85
[53] Brindha E, Rajasekaran R, Aruna P, Koteeswaran D and Ganesan S 2017 High wavenumber Raman spectroscopy in the characterization of urinary metabolites of normal subjects, oral premalignant and malignant patients *Spectrochim. Acta* A **171** 52–9
[54] Mo J, Zheng W, J H Low J, Ng J, Ilancheran A and Huang Z 2009 High wavenumber Raman spectroscopy for *in vivo* detection of cervical dysplasia *Anal. Chem.* **81** 8908–15
[55] Xu W, Ling X, Xiao J, Dresselhaus M S, Kong J, Xu H, Liu Z and Zhang J 2012 Surface enhanced Raman spectroscopy on a flat graphene surface *Proc. Natl Acad. Sci.* **109** 9281–6
[56] Zhu X, Shi L, Schmidt M S, Boisen A, Hansen O, Zi J, Xiao S and Mortensen N A 2013 Enhanced light–matter interactions in graphene-covered gold nanovoid arrays *Nano Lett.* **13** 4690–6